Chapter 3. AlGaAs/InGaAs Quantum Well Lasers on Si Substrates with InGaAs Intermediate Layers

3.1 Introduction

It has been recently reported that strained AlGaAs/InGaAs quantum well lasers grown on GaAs substrates, which are promising for new applications such as pumping Er^{3+}-doped optical fiber amplifiers at 980 nm[1-3], show very slow degradation rates and long lifetimes[4-12]. Waters and co-workers[7,9] have observed that strained AlGaAs/InGaAs SQW lasers on GaAs are significantly more resistant to <100> DLD propagation than AlGaAs/GaAs lasers on GaAs. Fukagai et al.[10] have reported that no <100> DLD was observed and DLDs grew in the <110> direction for the strained AlGaAs/InGaAs double quantum well (DQW) laser on GaAs. In addition, they have demonstrated that the <110> DLD growth velocity in the AlGaAs/InGaAs laser on GaAs was estimated to be ~1/100 of that for the <100> DLD growth velocity in the AlGaAs/GaAs laser on GaAs[10]. This suppressed <100> DLD growth is believed to result from the dislocation pinning due to the introduction of In in the GaAs active layer. Kirkby[13] has shown that dislocation motion can be drastically reduced by the incorporation of In (and other group-III or V impurities) into GaAs, which is similar to alloy hardening of metals[14]. To date, there has been only one demonstration of the increased lifetime for GaAs-based lasers on Si by replacing the conventional GaAs quantum well active layer with the InGaAs layer[15]. However, differences of degradation mechanism between AlGaAs/GaAs and AlGaAs/InGaAs quantum well lasers on Si have not been clarified. Furthermore, for the AlGaAs/InGaAs laser on Si, the relationship between reliability and residual stress in the InGaAs

active layer has not been also made clear.

In this chapter, the reliable AlGaAs/InGaAs SQW lasers on Si with InGaAs dislocation suppressing intermediate layers (InGaAs ILs) are demonstrated and the differences of degradation mechanism between AlGaAs/GaAs and AlGaAs/InGaAs SQW lasers on Si are also studied. This chapter is organized as follows: The epitaxial growth and fabrication process of the AlGaAs/InGaAs lasers on Si are described in section 3.2. In section 3.3, lasing characteristics of these lasers are presented. The reliability and degradation mechanism of the lasers are described in section 3.4. In section 3.5, increasing lifetime of the AlGaAs/InGaAs laser on Si by post-growth annealing is presented. This chapter is concluded in section 3.6.

3.2 Epitaxial Growth and Fabrication Process

Figure 3.1 shows a schematic cross-section of the AlGaAs/InGaAs SQW laser on Si with InGaAs IL. The 20-nm-thick n^+-$In_{0.08}Ga_{0.92}As$ IL was inserted between a 2.0-μm-thick n^+-GaAs buffer layer and a 1.0-μm-thick n-$Al_{0.7}Ga_{0.3}As$ lower cladding layer. A 70-nm-thick undoped $Al_{0.3}Ga_{0.7}As$ lower confining layer, various 9-nm-thick undoped $In_xGa_{1-x}As$ (x=0, 0.02, 0.07, 0.10) SQW active layer, a 70-nm-thick undoped $Al_{0.3}Ga_{0.7}As$ upper confining layer, a 1.0-μm-thick p-$Al_{0.7}Ga_{0.3}As$ upper cladding layer, and an 80-nm-thick p^+-GaAs contact layer were subsequently grown on the n-$Al_{0.7}Ga_{0.3}As$ lower cladding layer. Thermal cycle annealing was performed five times by varying the substrate temperature between 350 and 850 °C during the n^+-GaAs buffer layer growth. After the growth, the lasers were fabricated by defined 10-μm-wide oxide stripe opening to contact the p^+-GaAs layer. In order to compare the lasing characteristics, an

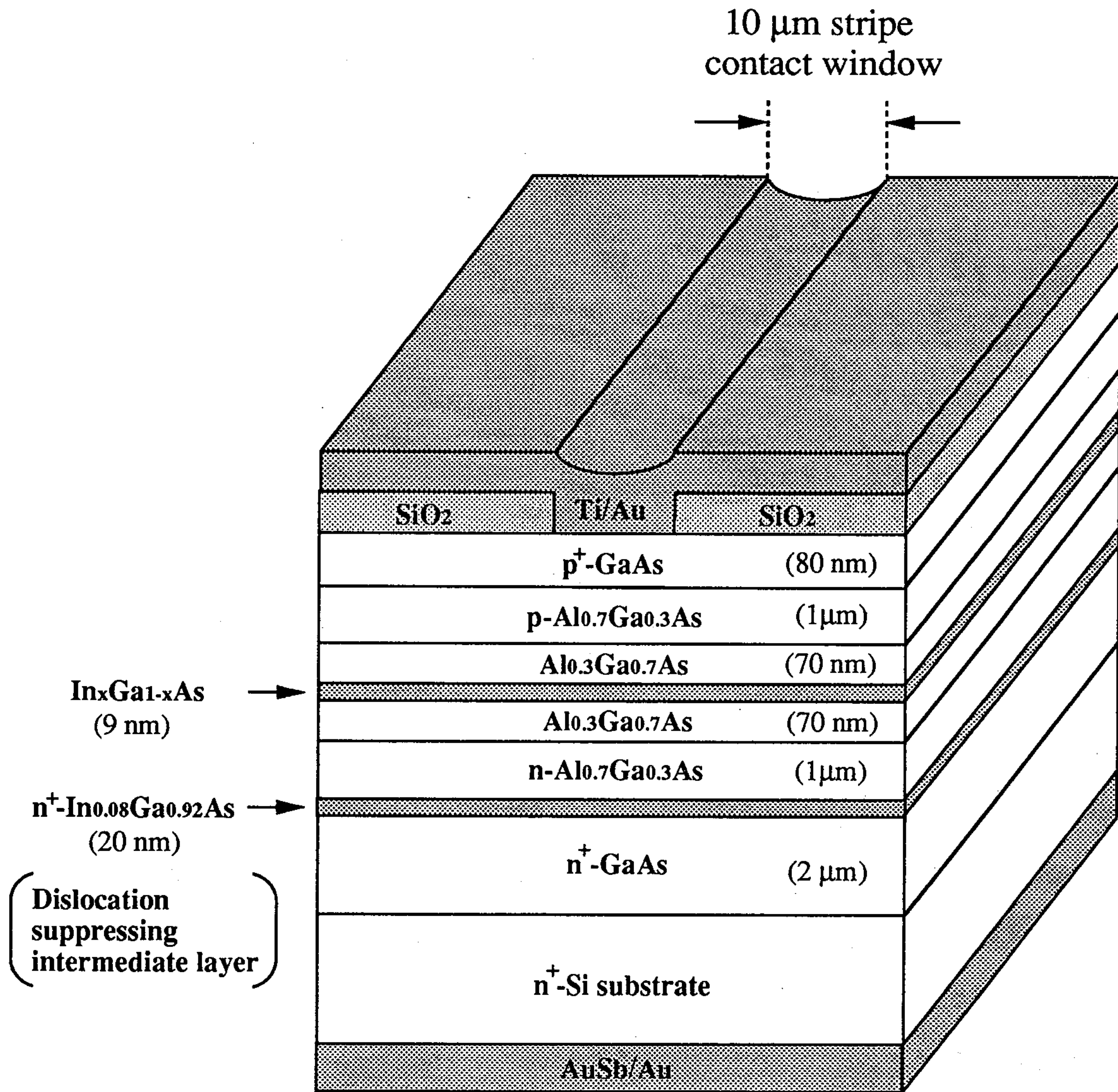

Fig. 3.1. Schematic cross-section of AlGaAs/InGaAs SQW laser on Si with InGaAs IL.

AlGaAs/GaAs SQW laser on GaAs and AlGaAs/$In_xGa_{1-x}As$ (x=0, 0.01, 0.07) SQW lasers on Si without InGaAs IL , which were similar laser structures described above, were also prepared.

Figure 3.2 shows variation of lattice constants of Si, GaAs, GaAs/Si, $In_{0.02}Ga_{0.98}As$ and $In_{0.07}Ga_{0.93}As$ during cooling-down from the growth temperature to room-temperature[16)]. The linear thermal expansion coefficients for these materials in the temperature range between 300 and 1000 K can be obtained from the slope of each line. During cooling from the growth temperature (~1000 K) to room-temperature (~300 K), the large thermal stress of ~2×10^9 dyn/cm^2 is generated in GaAs/Si by the difference in the thermal expansion coefficients between GaAs and Si. Therefore, the lattice constant of GaAs/Si increases from point A to B in Fig. 3.2 at the room-temperature. If the In content (x=0.02) in the $In_xGa_{1-x}As$ which is lattice-matched for the GaAs/Si at the middle temperature between 300 and 1000 K is chosen, the difference in the lattice constants between $In_{0.02}Ga_{0.98}As$ and GaAs/Si is -0.09 % at 300 K and +0.14 % at 1000 K, as shown in Fig. 3.2. Therefore, the thermally induced stress in the $In_{0.02}Ga_{0.98}As$ layer grown on GaAs/Si can be relieved without introduction of misfit dislocations. Even AlGaAs/GaAs laser structure on GaAs also has the lattice-mismatch of ~+0.14 %. On the other hand, the difference in the lattice constants between $In_{0.07}Ga_{0.93}As$ and GaAs/Si is +0.27 % at 300 K and +0.49 % at 1000 K. Thus, the misfit dislocations can be introduced in the $In_{0.07}Ga_{0.93}As$ layer grown on GaAs/Si if the $In_{0.07}Ga_{0.93}As$ layer is thicker than the critical thickness (hc).

Figure 3.3 shows the hc calculated for a GaAs/$In_xGa_{1-x}As$ single layer from the model of Matthews and Blakeslee[17)] and the model of People and Bean[18)]. The circles corresponding to the 9-nm-thick $In_xGa_{1-x}As$ (x=0, 0.01, 0.02, 0.07, 0.10) SQW active layers used in

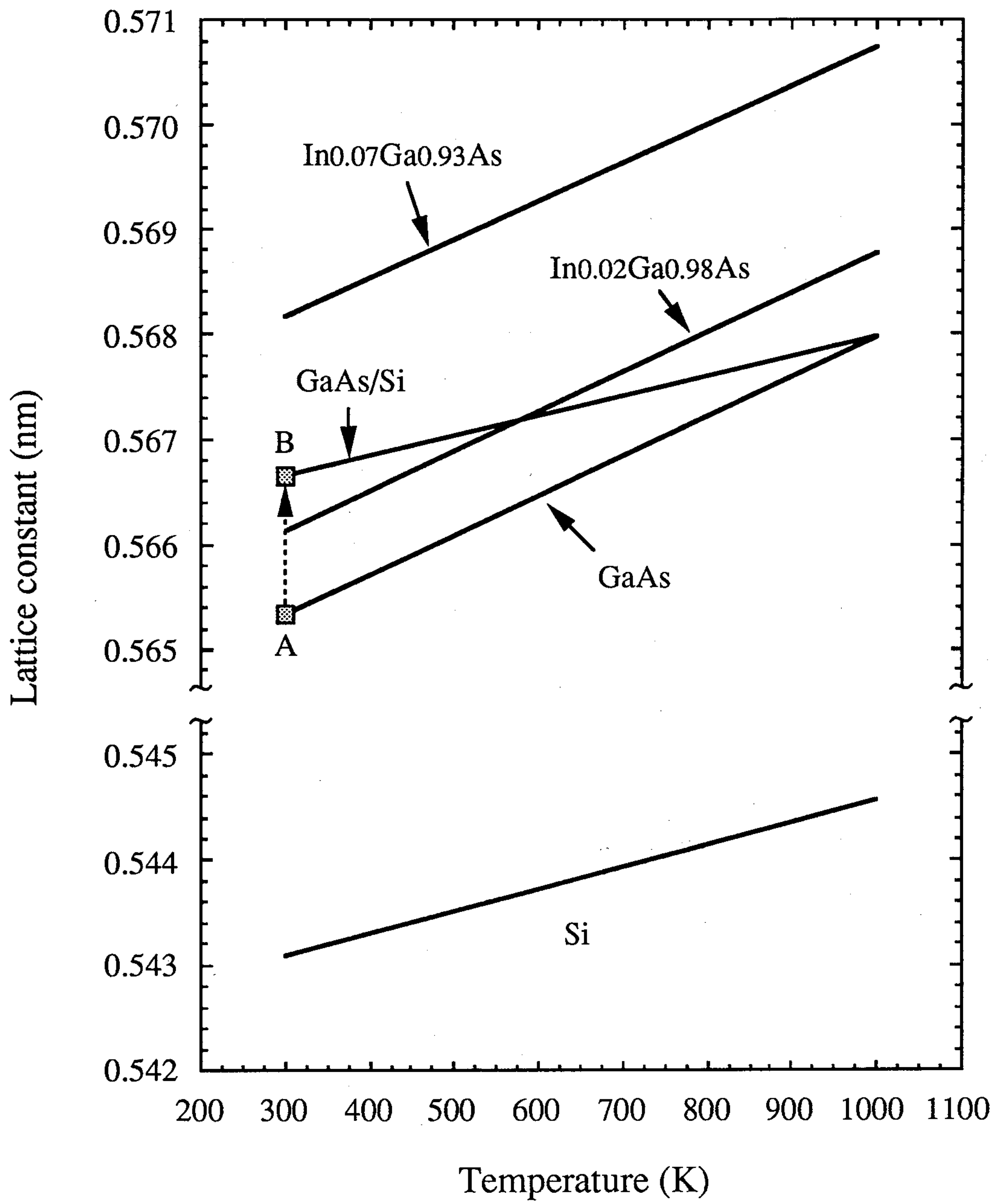

Fig. 3.2. Variation of lattice constants of Si, GaAs, GaAs/Si, $In_{0.02}Ga_{0.98}As$ and $In_{0.07}Ga_{0.93}As$ during cooling-down from the growth temperature to room-temperature[16].

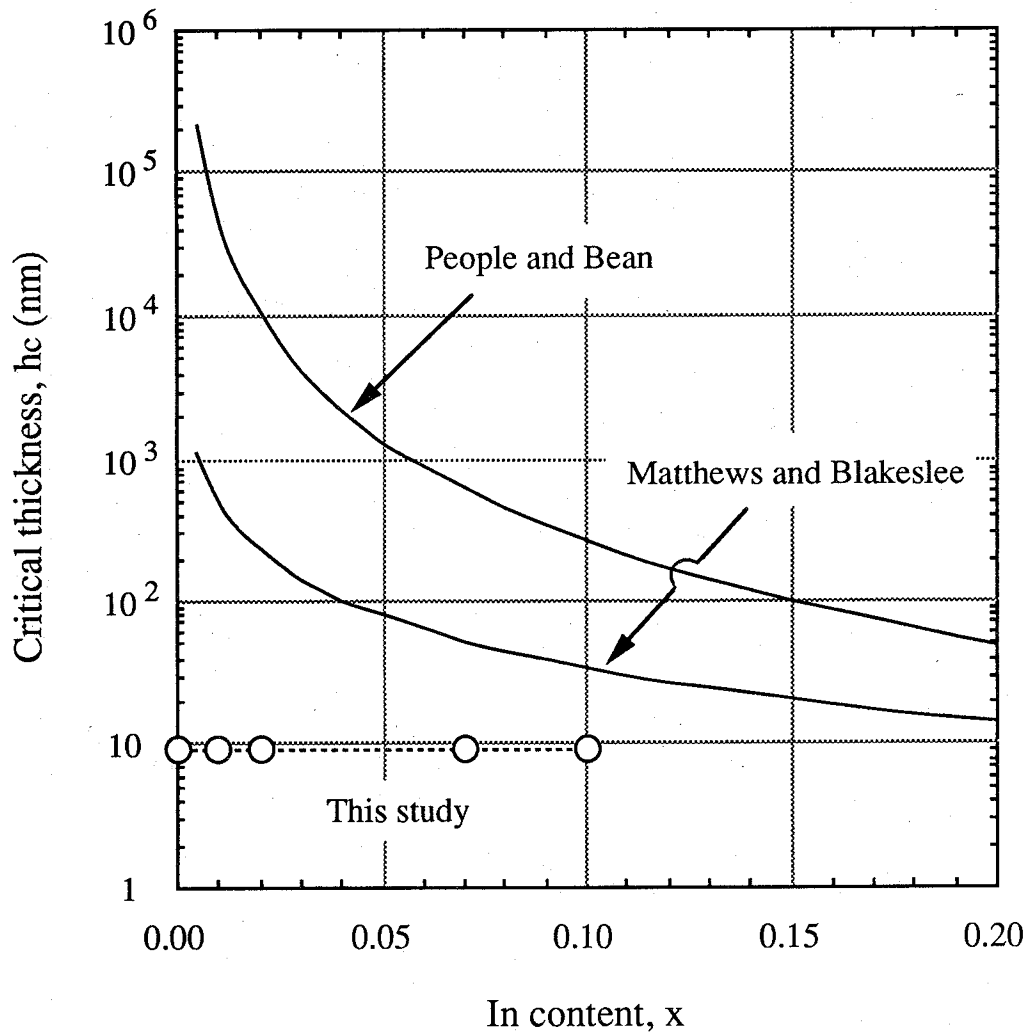

Fig. 3.3. Critical thichness calculated for a $GaAs/In_xGa_{1-x}As$ single layer from the model of Matthews and Blakeslee and the model of People and Bean.

this study are also shown. For all the active layers, the thickness is enough below the hc. Therefore, the lattice-mismatched strain in the active layers can be accommodated elastically without formation of misfit dislocations.

Under cw condition at room-temperature, the lasing characteristics such as polarization, threshold current density, emission wavelength, lasing characteristic parameters and reliability were studied[19-22]. In addition, the crystallinity of the active layers in the lasers was characterized by cathodoluminescence (CL) observations using a SEM (Topcon ABT-55).

3.3 Lasing Characteristics

3.3.1 Polarization

It is well known that the stress in the active layers of the lasers affects the polarization of the output light[23-28]. Therefore, the residual stress in the active layers can be relatively estimated from the degree of polarization (ρ). The degree of ρ is given by[23]

$$\rho = (L_{TE}-L_{TM})/(L_{TE}+L_{TM}), \qquad (3.1)$$

where L_{TE} and L_{TM} are the intensities of the transverse electric (TE) and transverse magnetic (TM) polarized output light, respectively. Therefore, ρ varies from +1 for completely TE polarized emission, to 0 for equal portions of TE and TM polarized light, and to -1 for completely TM polarized emission. Predominantly, TE and TM polarized emissions from the quantum well active layers are associated with electron-to-heavy hole and electron-to-light hole quantum state transitions, respectively.

Figure 3.4 shows a typical polarization of the AlGaAs/GaAs SQW laser on Si under cw condition at room-temperature. It is found that the lasing occurs in only the TE mode. In order to estimate the stress in the active layers, it is necessary to observe the spontaneous emission below threshold current (I_{th}) because of elimination of the dependence on mode reflectivity affecting polarization[23]. The dependence of ρ on the normalized current (I/I_{th}) for five kinds of lasers with ~400-μm-long cavity length (L) is shown in Fig. 3.5. The degree of ρ of a conventional AlGaAs/GaAs laser on Si is lower than that of an AlGaAs/GaAs laser on GaAs. This result indicates that the tensile stress in the active layer of the AlGaAs/GaAs laser on Si causes the light- and heavy-hole valence band quantum states to move closer together with increasing the TM polarized emission[29-33]. It is noticeable in Fig. 3.5 that the stress in the active layer can be changed from tensile to compressive stress with increasing the In content in the InGaAs active layer. The data indicates that the stress in the active layer of the AlGaAs/$In_{0.02}Ga_{0.98}As$ laser on Si with InGaAs IL can be relieved, which is equivalent to that of the AlGaAs/GaAs laser on GaAs. The AlGaAs/$In_{0.01}Ga_{0.99}As$ laser on Si without InGaAs IL has also the strain-relieved active layer. On the other hand, it was confirmed that the AlGaAs/$In_{0.07}Ga_{0.93}As$ laser on Si with InGaAs IL has a compressive stress in the active layer.

3.3.2 Threshold Current Density

In order to study the lasing characteristics, these lasers with various L were operated under cw condition at room-temperature. Figure 3.6 shows the relationship of J_{th} versus L for the AlGaAs/GaAs lasers on Si and AlGaAs/$In_xGa_{1-x}As$ (x=0.02, 0.07) lasers on Si with InGaAs ILs. For L=200-600 μm, the value of J_{th} of the

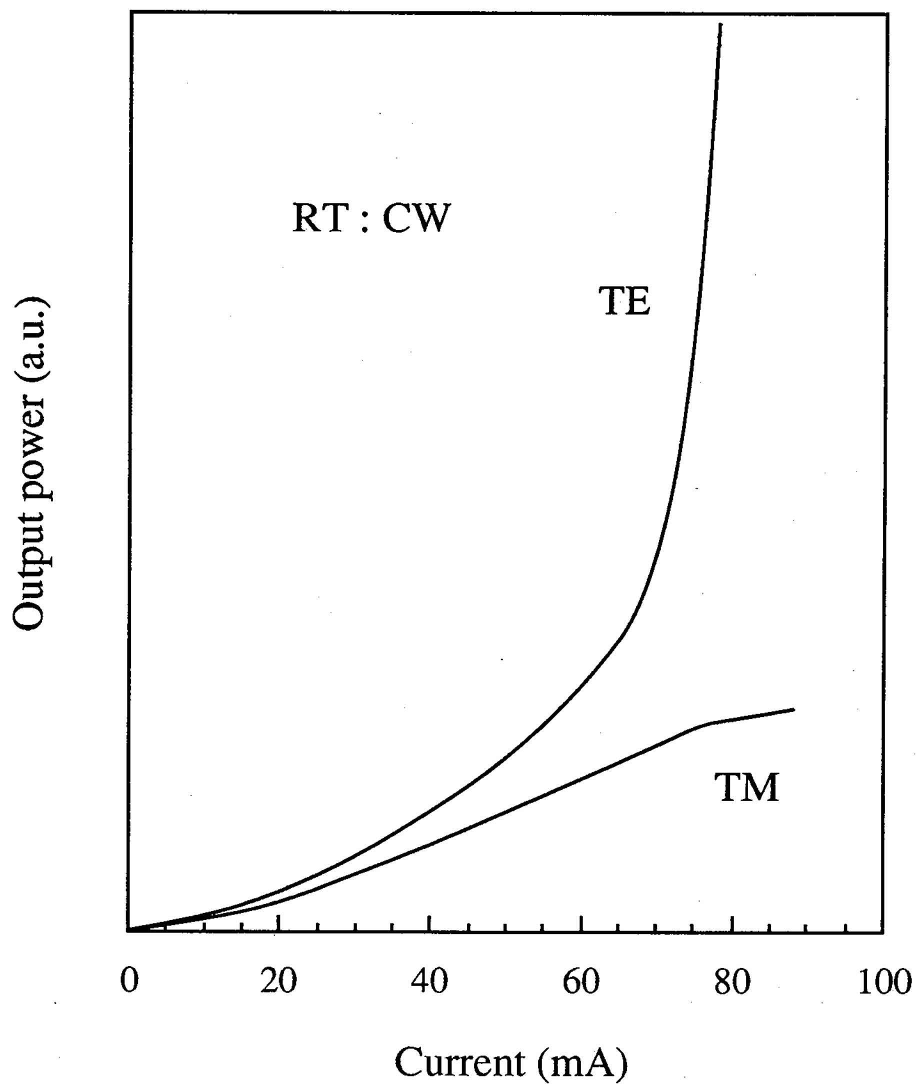

Fig. 3.4. Typical polarization of AlGaAs/GaAs SQW laser on Si under cw condition at room-temperature.

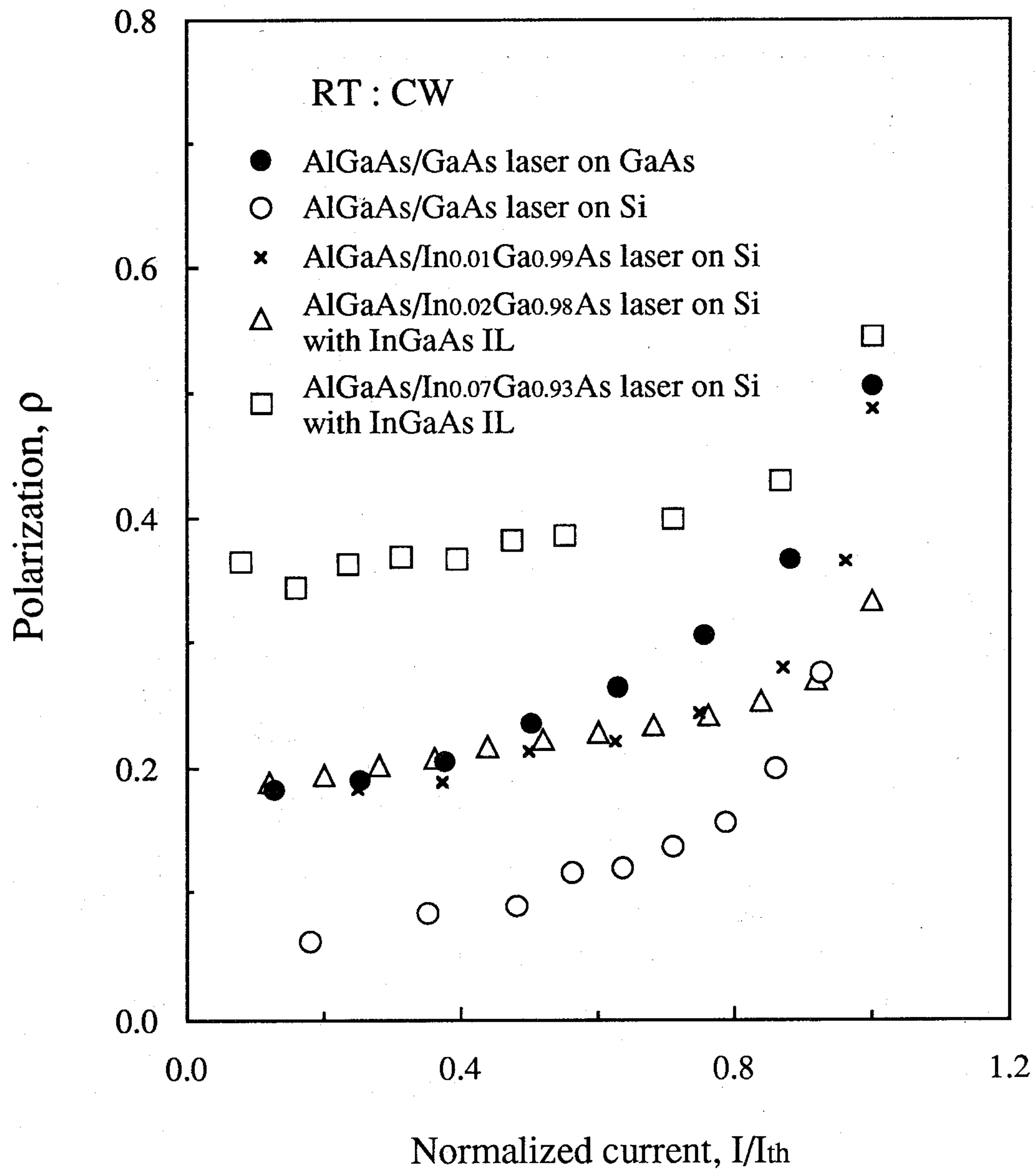

Fig. 3.5. Dependence of degree of polarization, ρ, on the normalized current (I/I_{th}).

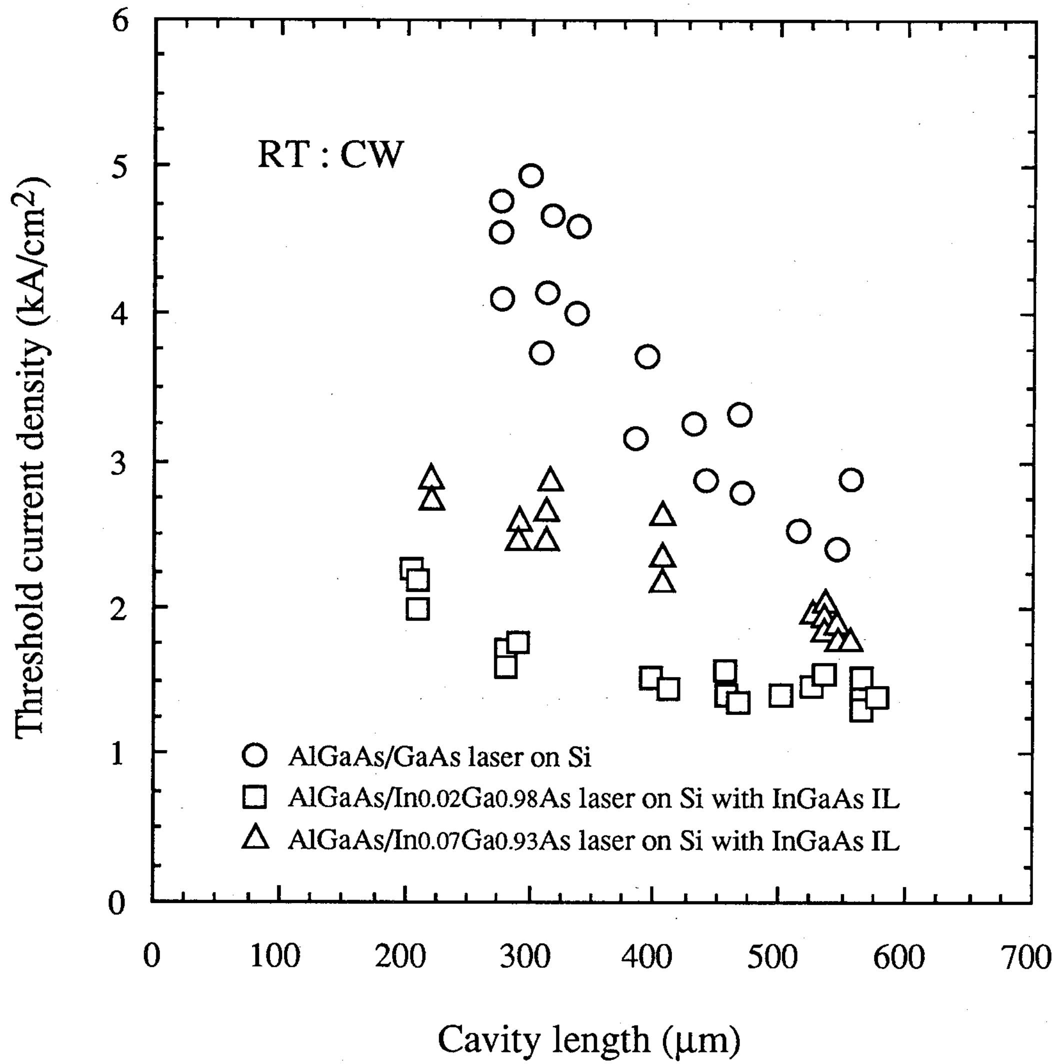

Fig. 3.6. Relationship of threshold current density versus cavity length for lasers on Si.

$AlGaAs/In_{0.02}Ga_{0.98}As$ lasers is lower than that of the AlGaAs/GaAs lasers. This result is the same as the dependence of J_{th} on the In content which was observed for AlGaAs/InGaAs lasers on GaAs[34-36]. It is also found that the value of J_{th} of the $AlGaAs/In_{0.07}Ga_{0.93}As$ lasers tends to be higher than that of the $AlGaAs/In_{0.02}Ga_{0.98}As$ lasers.

In order to characterize the crystallinity of the active layer in the $AlGaAs/In_{0.07}Ga_{0.93}As$ laser on Si with InGaAs IL, the CL observation was carried out using a SEM at low temperature (~130 K). The accelerated beam voltages were 20 and 30 kV. This CL observation was also carried out for the conventional AlGaAs/GaAs laser on Si without InGaAs IL and $AlGaAs/In_xGa_{1-x}As$ (x=0, 0.02, 0.10) lasers on Si with InGaAs ILs as references. Figure 3.7 shows the top-viewed CL images of the four kinds of lasers on Si. These images were taken at the wavelength (energy) of the each active layer. The nonradiative recombination regions at dislocations and the other defects can be seen as dark spots (DSs). The dark spot density (DSD) of the conventional AlGaAs/GaAs laser on Si is estimated to be $0.8\text{-}1.0\times10^{7}$ cm^{-2}. However, the value of this DSD may be lower than that of EPD by molten KOH etching, because it is possible that some of the DSs overlap with each other, making DSD lower than EPD[37]. The DSD is effectively reduced to $4\text{-}6\times10^{6}$ cm^{-2} for the AlGaAs/GaAs laser on Si with InGaAs IL due to the suppression of threading dislocations by introduction of InGaAs IL. For the $AlGaAs/In_{0.02}Ga_{0.98}As$ laser, the DSD is estimated to be $3\text{-}4\times10^{6}$ cm^{-2}. It is particularly noteworthy that the DLDs oriented towards the <110> direction can be clearly seen in the $AlGaAs/In_{0.07}Ga_{0.93}As$ and $AlGaAs/In_{0.10}Ga_{0.90}As$ lasers. Furthermore, it is found that the number of the <110> DLDs increased with increasing the In content in the InGaAs active layer. This

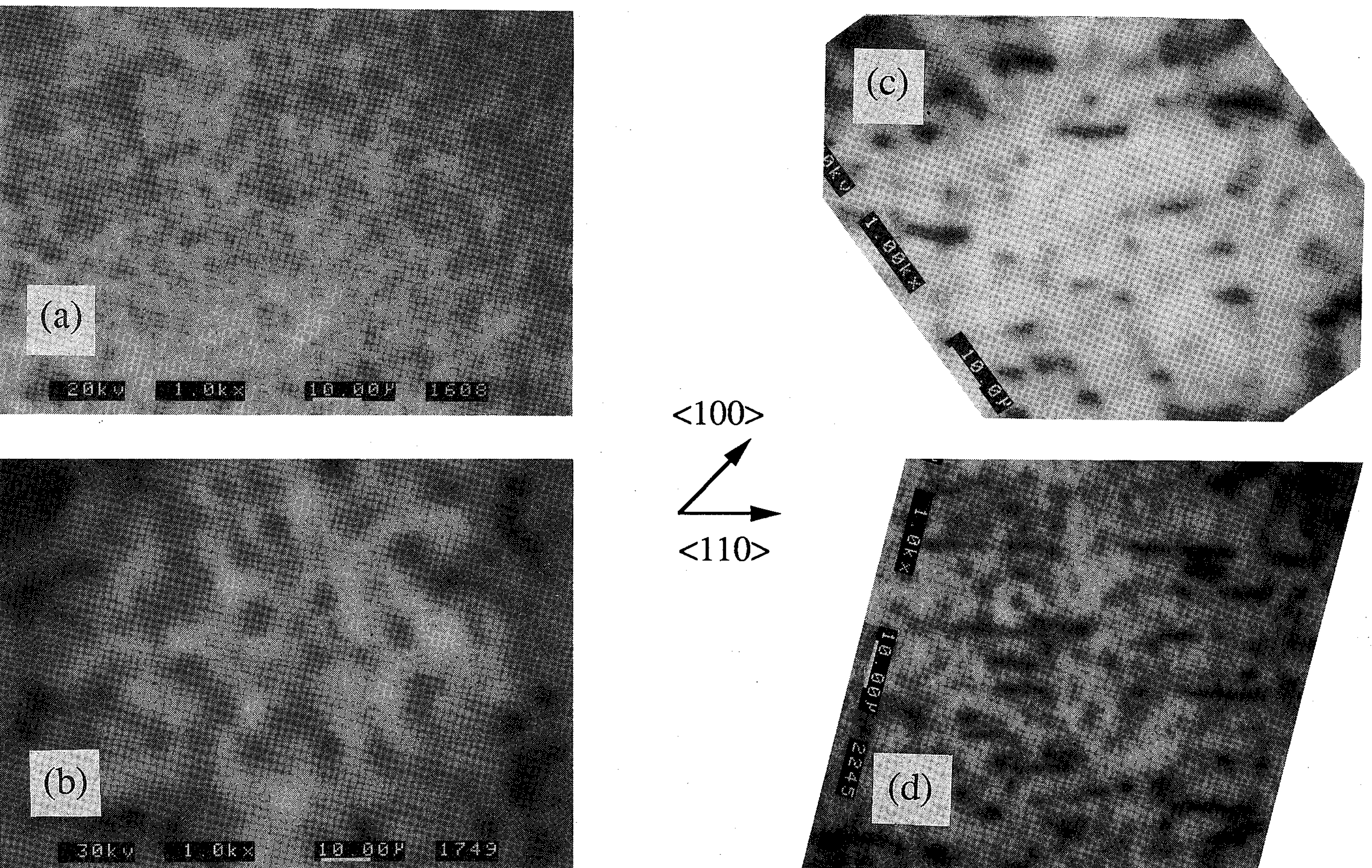

Fig. 3.7. CL images of the (a) AlGaAs/GaAs laser on Si without InGaAs IL, (b) AlGaAs/$In_{0.02}Ga_{0.98}As$, (c) AlGaAs/$In_{0.07}Ga_{0.93}As$ and (d) AlGaAs/$In_{0.10}Ga_{0.90}As$ lasers on Si with InGaAs ILs.

result clearly suggests that the higher strain associated with the increase of the In content enhances the bend of threading dislocations in the active layer[29,38,39], resulting in the raise in the J_{th} due to the increase of nonradiative recombination centers[15], as shown in Fig. 3.6.

3.3.3 Emission Wavelength

The emission wavelengths of the $AlGaAs/In_xGa_{1-x}As$ (x=0, 0.02, 0.07) lasers on Si with InGaAs IL were measured. In this measurement, the ~400-μm-long cavities were used for these lasers, because short cavities (L<300 μm) show a sharp decrease in the wavelength due to the emission shifts from n=1 to n=2 quantum state transition in the quantum well. This shift in the emission wavelength with decreasing L are the result of saturation of the available quantum well gain[36,40]. It was confirmed that the emission wavelength monotonously increased from ~845 nm for the AlGaAs/GaAs laser, to ~865 nm for the $AlGaAs/In_{0.02}Ga_{0.98}As$ laser, and to ~885 nm for the $AlGaAs/In_{0.07}Ga_{0.93}As$ laser. This increasing wavelength is associated with the decrease of InGaAs band-gap energy with increasing In content[34,35]. These wavelengths are from n=1 transition. For the $AlGaAs/In_{0.10}Ga_{0.90}As$ laser on Si with InGaAs IL, however, the emission wavelength from n=1 transition could not be measured and the laser was operated at ~855 nm from n=2 transition. The reason is thought to be that the increase of J_{th} due to the very poor crystallinity of the active layer [as shown in Fig. 3.7(d)] resulted in the difficulty of the n=1 transition.

3.3.4 Lasing-Characteristic Parameters

For the AlGaAs/GaAs lasers on Si with and without InGaAs IL, and $AlGaAs/In_xGa_{1-x}As$ (x=0.02, 0,07) lasers on Si with InGaAs ILs,

the lasing-characteristic parameters such as η_i, α_i, β and J_0 were determined by eqs. (2.1) and (2.2), and are summarized in Table III.I. It was assumed that Γ is 0.027 for the SQW laser[41]. An AlGaAs/GaAs SQW laser on GaAs was also characterized as a reference.

The value of η_i seems to be considerably associated with the crystallinity of the active layer. That of η_i increased from 61 % for the conventional AlGaAs/GaAs laser without InGaAs IL, to 77 % for the AlGaAs/GaAs laser with InGaAs IL, and to 81 % for the AlGaAs/$In_{0.02}Ga_{0.98}As$ laser. These improvements are certainly caused by InGaAs IL which improves the crystallinity of the active layer, as shown in Fig. 3.7(b). However, it decreased to 72 % for the AlGaAs/$In_{0.07}Ga_{0.93}As$ laser. This is probably due to the increased nonradiative recombination centers related to the generation of bent threading dislocations (<110> DLDs) for the AlGaAs/$In_{0.07}Ga_{0.93}As$ laser, as shown in Fig. 3.7(c).

The value of α_i was reduced from 26 cm^{-1} for the conventional AlGaAs/GaAs laser, to 15 cm^{-1} for the AlGaAs/GaAs laser with InGaAs IL, and to 17 cm^{-1} for the AlGaAs/$In_{0.02}Ga_{0.98}As$ laser. For the AlGaAs/$In_{0.07}Ga_{0.93}As$ laser, it decreased to 19 cm^{-1}. However, this reason is not understood yet.

Additionally, it was found that the β was associated with the In content in the InGaAs active layer. The value of β was 1.4 cm/A and 1.7 cm/A for the AlGaAs/GaAs lasers on Si with and without InGaAs IL, respectively. It increased from 1.7 cm/A for the AlGaAs/$In_{0.02}Ga_{0.98}As$ laser to 2.7 cm/A for the AlGaAs/$In_{0.07}Ga_{0.93}As$ laser. In particular, it is noticeable that the β of 2.7 cm/A is larger than that of 2.0 cm/A for the AlGaAs/GaAs laser on GaAs. This improvement seems to have been caused by the compressive stress in the active layer, as shown in Fig. 3.5. The similar improvement of β has been observed for the

Table III.I. Summary of lasing-characteristic parameters for lasers.

	η_i (%)	α_i (cm^{-1})	β (cm/A)	J_0 (A/cm^2)
AlGaAs/GaAs laser on GaAs	87	21	2.0	100
AlGaAs/GaAs laser on Si	61	26	1.7	270
AlGaAs/GaAs laser on Si with InGaAs IL	77	15	1.4	280
AlGaAs/$In_{0.02}Ga_{0.98}As$ laser on Si with InGaAs IL	81	17	1.7	250
AlGaAs/$In_{0.07}Ga_{0.93}As$ laser on Si with InGaAs IL	72	19	2.7	410

AlGaAs/InGaAs lasers on GaAs[36]. This improvement has been also theoretically explained as a result of the additional strain-induced separation of energies of the the various valence band quantum state transitions[42-45].

In addition, the value of J_0 is much larger for the AlGaAs/$In_{0.07}Ga_{0.93}As$ laser than for the AlGaAs/$In_{0.02}Ga_{0.98}As$ laser. Although this is the opposite tendency observed for the AlGaAs/InGaAs lasers on GaAs[36,46,47], the reason is thought to be the increase of the nonradiative recombination current at the bent threading dislocations for the AlGaAs/$In_{0.07}Ga_{0.93}As$ laser.

3.4 Reliability and Degradation Mechanism

3.4.1 Reliability

In order to study the reliability of these lasers, the cw aging tests were carried out at a constant output power of 1 mW/facet under APC operation at room-temperature. The conventional AlGaAs/GaAs laser on Si showed very rapid degradation only in a few minutes (as shown in Fig. 2.2) because the laser has a high DSD of $0.8-1.0\times10^7$ cm^{-2} and a large tensile stress in the active layer[48,49]. The AlGaAs/GaAs laser on Si with InGaAs IL also degraded very rapidly as well as the the AlGaAs/GaAs laser on Si without InGaAs IL. This result indicates that the reduction of DSD from $0.8-1.0\times10^7$ to $4-6\times10^6$ cm^{-2} in the GaAs active layers, which was caused by inserting the InGaAs IL, is hardly effective in increasing the lifetime of lasers on Si. In addition, the AlGaAs/$In_{0.01}Ga_{0.99}As$ and AlGaAs/$In_{0.07}Ga_{0.93}As$ lasers on Si without InGaAs ILs also showed rapid degradation within a few minutes. In particular, the rapid degradation of the stress-relieved AlGaAs/$In_{0.01}Ga_{0.99}As$ laser seems to show that the relief of stress

in the active layer with high DSD (~10^7 cm^{-2}) is scarcely effective in improving the reliability.

Figure 3.8 shows the results from the aging tests at room-temperature for the several AlGaAs/$In_{0.02}Ga_{0.98}As$ and AlGaAs/$In_{0.07}Ga_{0.93}As$ lasers on Si with InGaAs ILs. For the stress-relieved AlGaAs/$In_{0.02}Ga_{0.98}As$ lasers, the lifetimes reaching 500 mA were ~40, 50 and 85 min. For the longest lifetime of ~85 min, the current increased at a rate of ~65 mA/h in the first 60 min, by ~230 mA/h in the next 15 min and then the laser showed a sharp increase in the degradation rate with time, which presumably resulted from the propagation of DLDs. On the other hand, despite the higher J_{th} of the AlGaAs/$In_{0.07}Ga_{0.93}As$ laser than that of the AlGaAs/$In_{0.02}Ga_{0.98}As$ laser (as shown in Fig. 3.6), the lifetimes of the AlGaAs/$In_{0.07}Ga_{0.93}As$ lasers were ~70, 80 and 105 min in which the latter two lasers showed gradual degradation without the sharp increase of current. These results suggest that the reduction of DSD by the InGaAs IL and the dislocation pinning by the InGaAs active layer are required to realize the reliable GaAs-based lasers on Si.

3.4.2 Degradation Mechanism by EL Observation

Using EL topography, the degradation mechanisms of the AlGaAs/$In_{0.02}Ga_{0.98}As$ and AlGaAs/$In_{0.07}Ga_{0.93}As$ lasers on Si with InGaAs ILs were investigated.

Figure 3.9 shows typical EL topographs of the AlGaAs/$In_{0.02}Ga_{0.98}As$ laser under dc operation at a constant current density of 1.0 kA/cm^2 and temperature of 20 °C. A DS originating from a pre-existing defect was observed before degradation [Fig. 3.9(a)]. At the first degradation stage after 35 min [Fig. 3.9(b)], one <100> DLD and many DSs were generated. In the next stage [Fig.

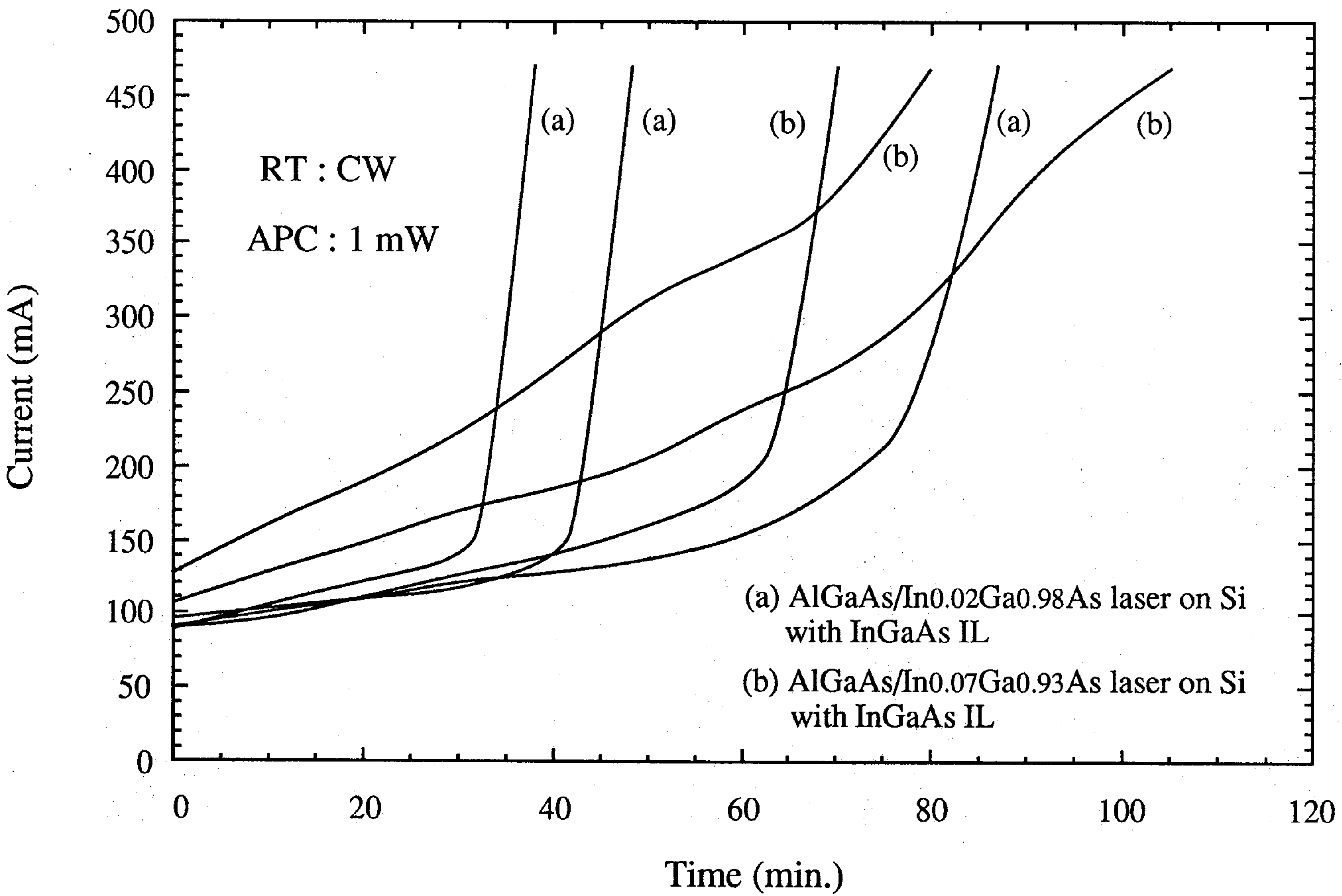

Fig. 3.8. Results from the APC aging tests under cw condition at room-temperature for the $AlGaAs/In_{0.02}Ga_{0.98}As$ and $AlGaAs/In_{0.07}Ga_{0.93}As$ lasers on Si with InGaAs ILs.

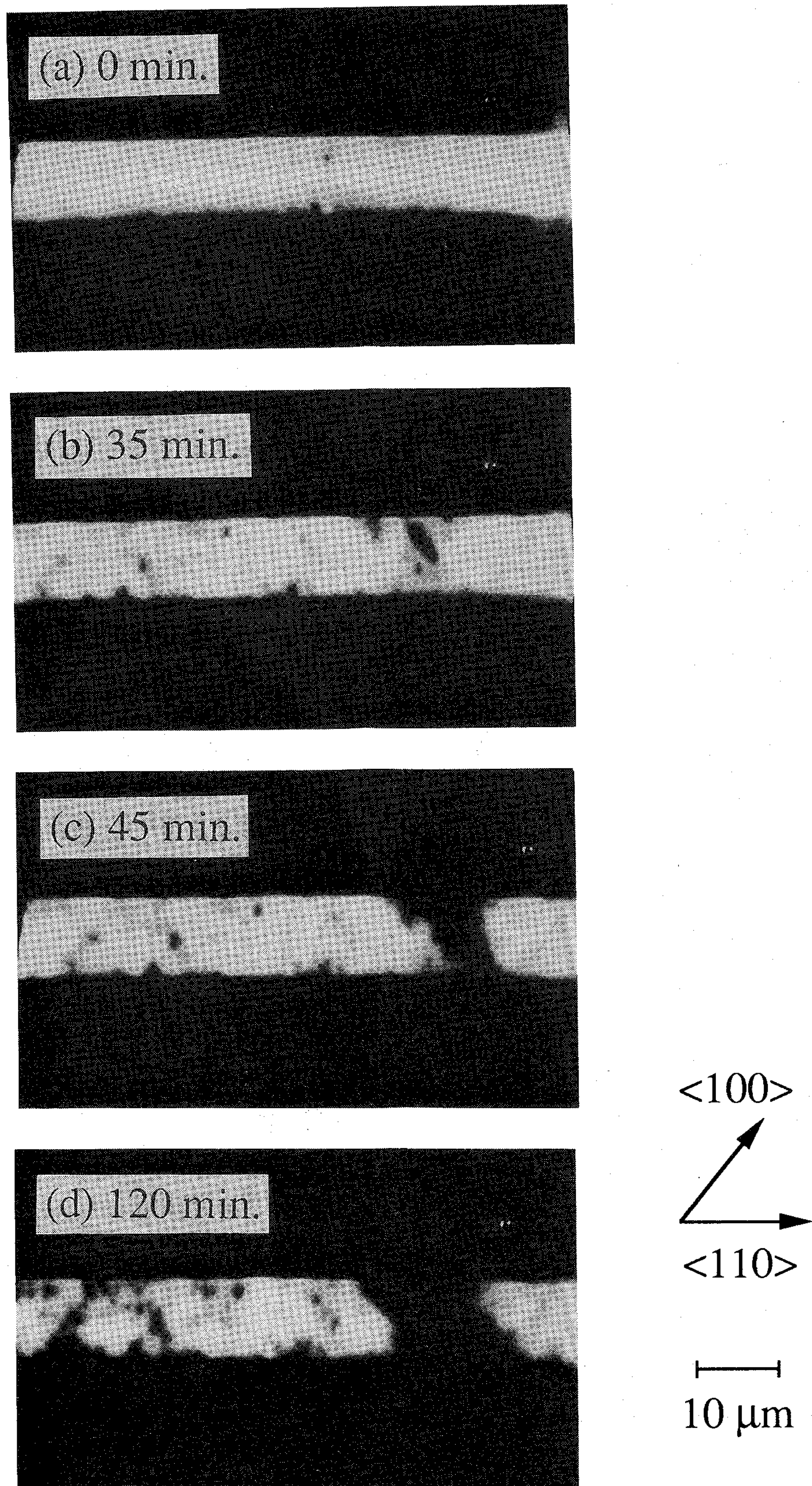

Fig. 3.9. Typical magnified EL topographs of the AlGaAs/$In_{0.02}Ga_{0.98}As$ laser on Si after (a) 0, (b) 35, (c) 45 and (d) 120 min under dc operation at a constant current density of 1.0 kA/cm^2 and temperature of 20 °C.

3.9(c)], the DLD extended towards both <100> and <110> directions in the active region. After 120 min [Fig. 3.9(d)], the DLD growth was enhanced towards <110> direction, and each DSs were broad in the vicinity of its originating defects which resulted from the formation of dislocation loops and dipoles at the threading dislocations[50,51). Compared with the degradation of an AlGaAs/GaAs laser on Si (as shown in Fig. 2.9), the generation and growth of DSs are particularly remarkable. This seems to indicate that the DLD formation is somewhat suppressed by the dislocation pinning in the InGaAs active layer[7,9,10,12,13).

Figure 3.10 shows typical EL topographs of the AlGaAs/$In_{0.07}Ga_{0.93}As$ laser under dc operation at a constant current density of 1.0 kA/cm^2 and temperature of 20 °C. As the EL observation was just started [Fig. 3.10(a)], several pre-existing DSs and <110> DLDs which are bent dislocations [as shown in Fig. 3.7(c)] were observed. In the following stage [Fig. 3.10(b)], one <100> DLD was generated from one DS in the center of the active region. In the subsequent stages [Figs. 3.10(c) and 3.10(d)], the DLD extended toward the edge of the active region. The growth of pre-existing <110> DLDs was not clearly observed after 76 min.

Figure 3.11 shows the dependence of the <100> DLD growth velocity on the injected current density for the AlGaAs/$In_{0.02}Ga_{0.98}As$ and AlGaAs/$In_{0.07}Ga_{0.93}As$ lasers at 20 °C. The data of AlGaAs/GaAs laser on Si (as shown in Fig. 2.10) was replotted in Fig. 3.11 as a reference. It was found that <100> DLD growth velocity (V) for the AlGaAs/GaAs laser was most strongly dependent on the injected current density (J), and the relationship between V and J for this laser was estimated as $V \propto J^{1.55}$. In contrast, the DLD growth velocity was reduced to $V \propto J^{1.51}$ for the AlGaAs/$In_{0.02}Ga_{0.98}As$ laser. For the AlGaAs/$In_{0.07}Ga_{0.93}As$ laser,

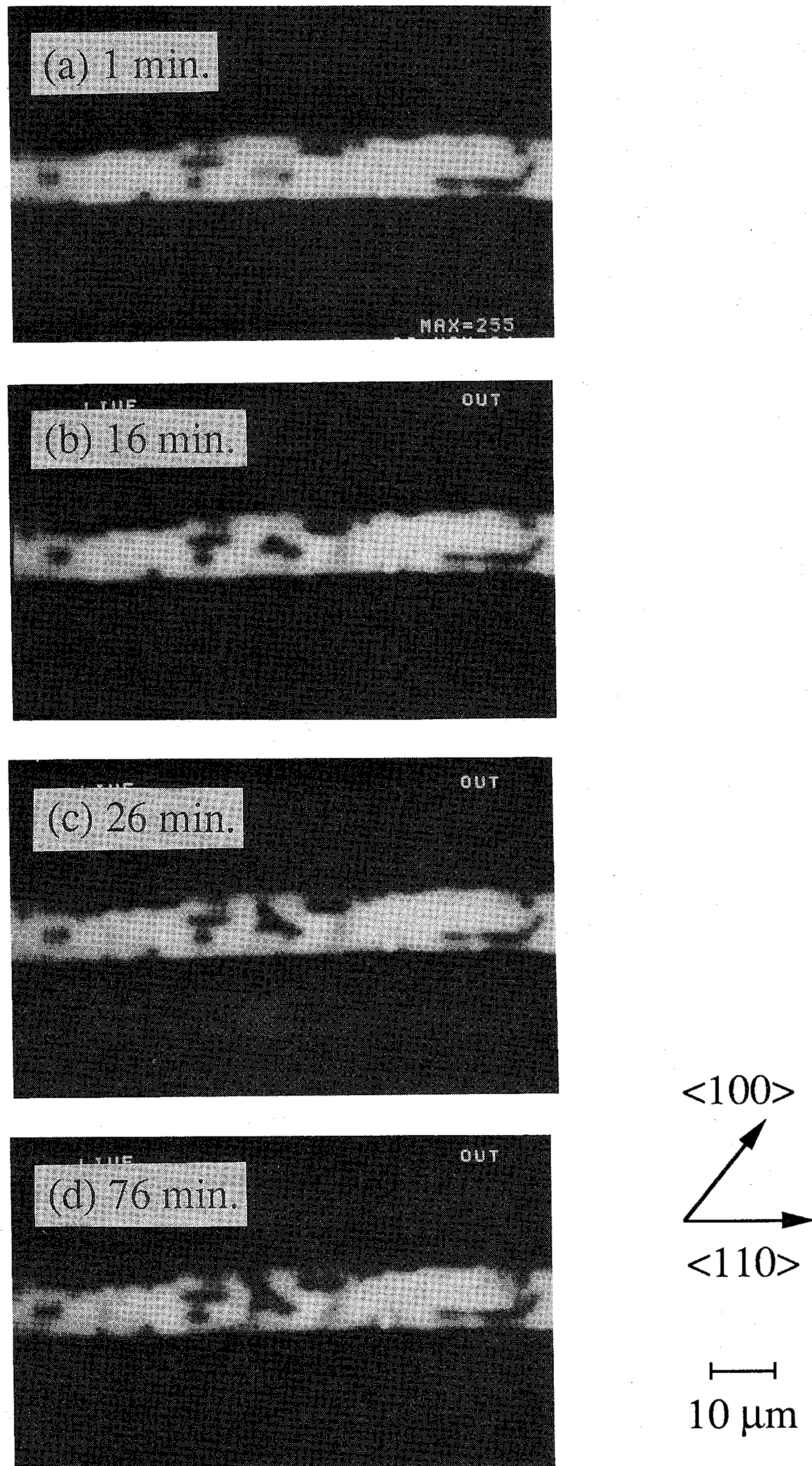

Fig. 3.10. Typical magnified EL topographs of the AlGaAs/$In_{0.07}Ga_{0.93}As$ laser on Si after (a) 1, (b) 16, (c) 26 and (d) 76 min under dc operation at a constant current density of 1.0 kA/cm^2 and temperature of 20 °C.

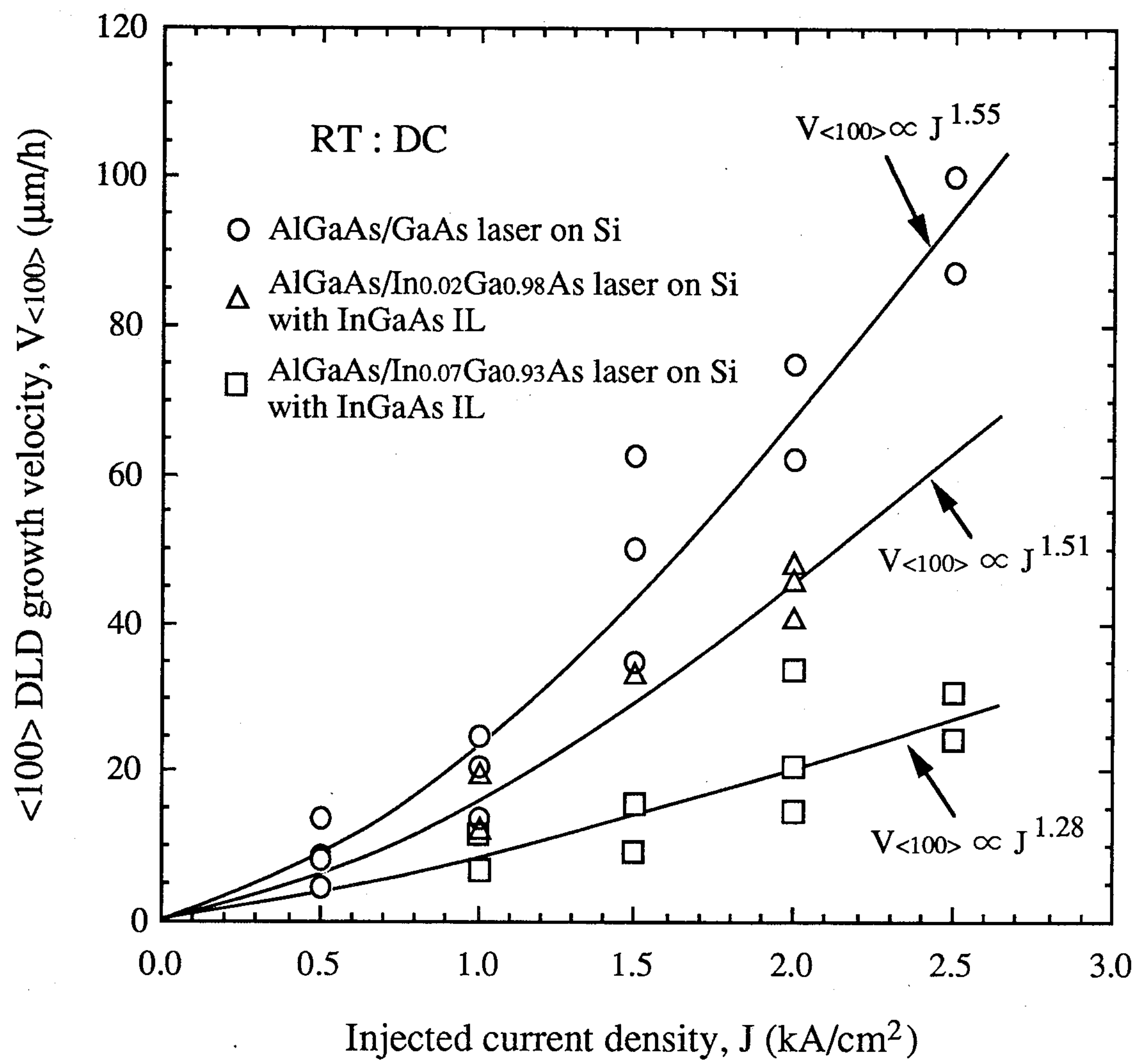

Fig. 3.11. Dependence of <100> DLD growth velocity on the injected current density for the lasers on Si.

the growth velocity was drastically reduced to $V \propto J^{1.28}$. For example, the value of V at J=2.0 kA/cm^2 was reduced from ~65 μm/h for the AlGaAs/GaAs laser, to ~45 μm/h for the AlGaAs/$In_{0.02}Ga_{0.98}As$ laser, and to ~20 μm/h for the AlGaAs/$In_{0.07}Ga_{0.93}As$ laser. These results indicate that the degradation mechanism related to <100> DLDs of the AlGaAs/InGaAs lasers on Si with InGaAs ILs is basically the same as that of the AlGaAs/GaAs laser on Si, but the increasing lifetimes of the AlGaAs/InGaAs lasers were caused by the reduction of the DLD growth velocity due to dislocation pinning in the InGaAs active layer[7,10]. After all, for the AlGaAs/InGaAs lasers on Si with InGaAs ILs, it seems that the dislocation pinning by higher In content (x=0.07) in the InGaAs active layer has a more attractive potential of improving the reliability rather than low (stress-relieved) In content (x=0.02).

3.5 Increased Lifetime of AlGaAs/InGaAs Laser on Si by Post-Growth Annealing

It has been reported that post-growth annealing is effective in improving the crystallinity of the GaAs/Si[52-54]. Therefore, the post-growth annealing was performed for the conventional AlGaAs/GaAs laser on Si and AlGaAs/$In_xGa_{1-x}As$ (x=0.02, 0.07) lasers on Si with InGaAs ILs. The processes of the post-growth annealing were as follows: A 0.1-μm-thick SiO_2 cap layer was deposited on the surface of each samples in order to prevent As atom detachment from the surface. Next, the samples were loaded into MOCVD reactor and annealed at 750 °C for 1 h in an AsH_3 atmosphere.

In order to study the crystallinity of the active layers in the post-growth annealed lasers, the CL observation was carried out at low-temperature. For the AlGaAs/GaAs laser, the improvement of

crystallinity was hardly observed. On the other hand, the remarkable improvement was particularly observed for the AlGaAs/$In_{0.07}Ga_{0.93}As$ laser. Figure 3.12 shows a CL image of the AlGaAs/$In_{0.07}Ga_{0.93}As$ laser after post-growth annealing. Compared with that of the laser before annealing as shown in Fig. 3.7(c), it can be seen that all <110> DLDs successfully vanished. This improvement is thought to be a result of the reduced bent threading dislocations, which resulted from the migration and interaction of the dislocations due to post-growth annealing.

The conventional 10-μm-wide oxide stripe contact lasers were fabricated from the annealed samples in order to investigate the lasing characteristics. All three kinds of lasers were operated under cw condition at room-temperature. Figure 3.13 shows a typical L-I characteristic of a post-growth annealed AlGaAs/$In_{0.07}Ga_{0.93}As$ laser on Si with InGaAs IL under cw condition at room-temperature . This laser with 600-μm-long cavity exhibited the I_{th} of 73 mA and the η_d of 21 %. The emission wavelength was also ~875 nm. For the annealed AlGaAs/$In_{0.02}Ga_{0.98}As$ and AlGaAs/$In_{0.07}Ga_{0.93}As$ lasers, the η_i was estimated by eq. (2.2). The value of η_i for the AlGaAs/$In_{0.02}Ga_{0.98}As$ laser was increased from 81 to 85 % by post-growth annealing. For the AlGaAs/$In_{0.07}Ga_{0.93}As$ laser, that of η_i was remarkably increased from 72 to 82 % by the annealing. However, the value of η_i was not changed for the AlGaAs/GaAs laser. These results correspond to the results of crystallinity of the active layers observed by CL.

The AlGaAs/GaAs lasers with and without the annealing degraded very rapidly within a few minutes. On the other hand, several annealed AlGaAs/$In_{0.02}Ga_{0.98}As$ and AlGaAs/$In_{0.07}Ga_{0.93}As$ lasers showed slow degradations and long lifetimes, as shown in Fig. 3.14. For the annealed AlGaAs/$In_{0.02}Ga_{0.98}As$ laser, the longest lifetime

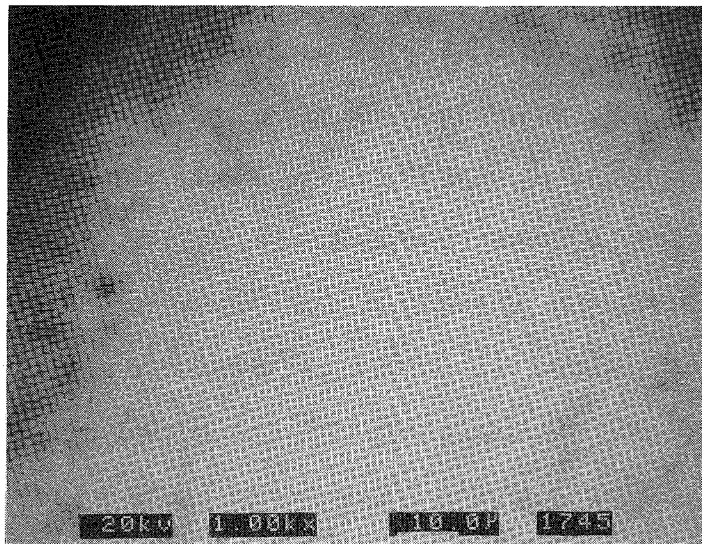

Fig. 3.12. CL image of the AlGaAs/$In_{0.07}Ga_{0.93}As$ laser on Si after post-growth annealing.

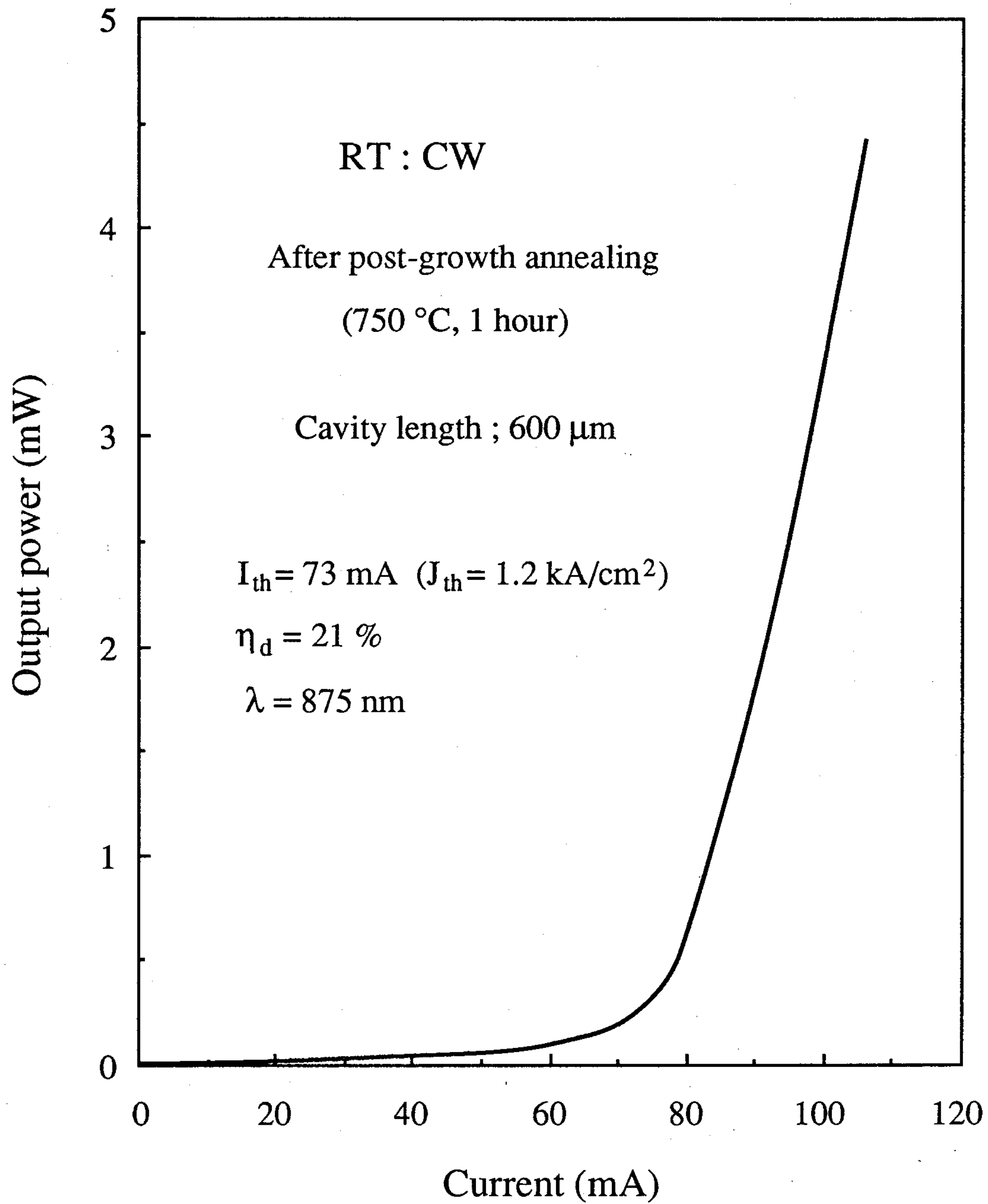

Fig. 3.13. Typical L-I characteristic of a post-growth annealed AlGaAs/$In_{0.07}Ga_{0.93}As$ laser on Si with InGaAs IL under cw condition at room-temperature.

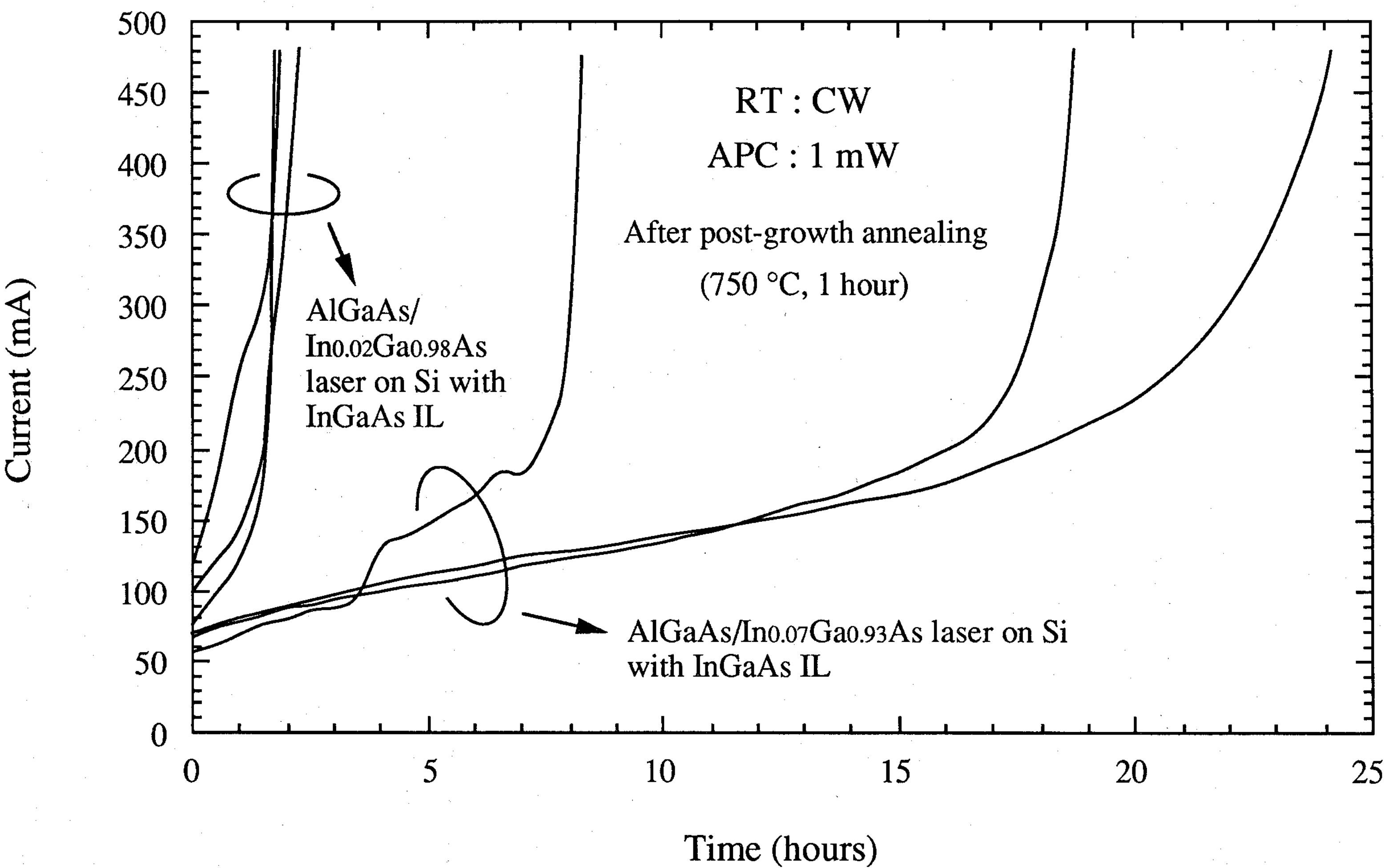

Fig. 3.14. Results from the APC aging tests under cw condition at room-temperature for the post-growth annealed AlGaAs/$In_{0.02}Ga_{0.98}As$ and AlGaAs/$In_{0.07}Ga_{0.93}As$ lasers on Si with InGaAs ILs.

was ~2.3 h which was ~1.6 times as long as the longest lifetime of ~87 min obtained from this laser before annealing. Furthermore, the longest lifetime obtained in this study was ~24 h for the annealed AlGaAs/$In_{0.07}Ga_{0.93}As$ laser (as shown in Fig. 3.13). In this case, the current increased at a rate of ~10 mA/h in the first 3 h, by ~6 mA/h after 15 h, by ~14 mA/h after 20 h, and then the laser showed a sharp increase in the degradation rate with time. This lifetime of ~24 h was ~14 times as long as the longest lifetime of ~105 min recorded from this laser before annealing. These results are believed to have been arisen from the improvement of crystallinity in the InGaAs active layers by post-growth annealing.

In order to investigate the degradation mechanism of the long-life AlGaAs/$In_{0.07}Ga_{0.93}As$ laser, the top-viewed EL observation was carried out under dc condition at a constant current density of 1.5 kA/cm^2 and temperature of 20 °C. Figure 3.15 shows typical EL topographs of an annealed AlGaAs/$In_{0.07}Ga_{0.93}As$ laser. A dark region extending towards the <110> direction (perpendicular to the stripe direction) was observed in the first degradation stage [Fig. 3.15(a)]. In the next stage after 1 h [Fig. 3.15(b)], several <110> DLDs were generated. In the subsequent stage [Figs. 3.15(c) and 3.15(d)], the <110> DLDs were grown, and many DSs were generated and some of them were transformed to <110> DLDs. This <110> DLD growth velocity was estimated to be ~6 μm/h at J=1.5 kA/cm^2, which is slower than the <100> DLD growth velocity of ~15 μm/h at the same value of J for this laser before annealing (as shown in Fig. 3.12). This degradation mechanism related to <110> DLDs is completely different from that mainly related to <100> DLDs observed in the other lasers on Si as shown in Figs. 2.9, 3.9 and 3.10. The result obtained from this EL observation indicates that the drastically increased lifetime of the annealed AlGaAs/$In_{0.07}Ga_{0.93}As$ laser was

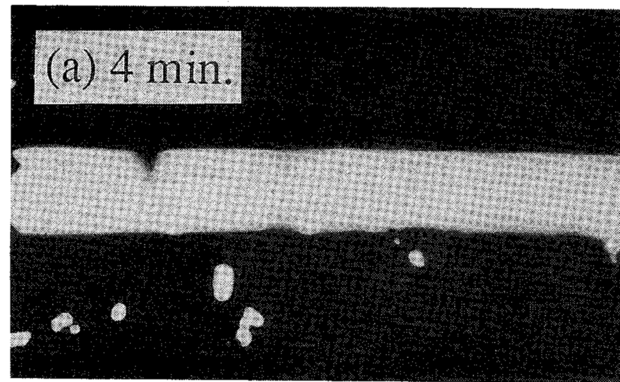

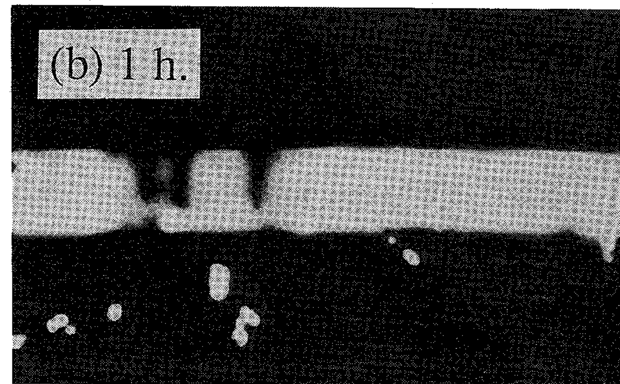

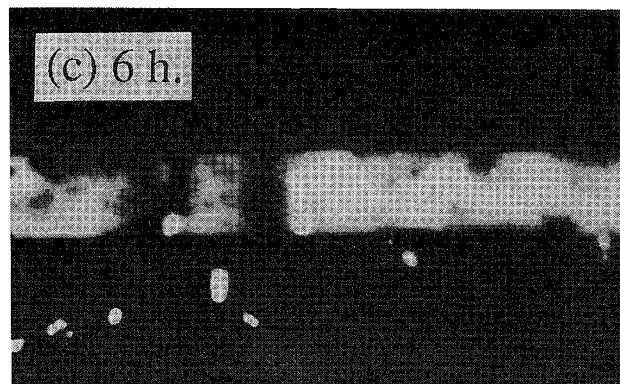

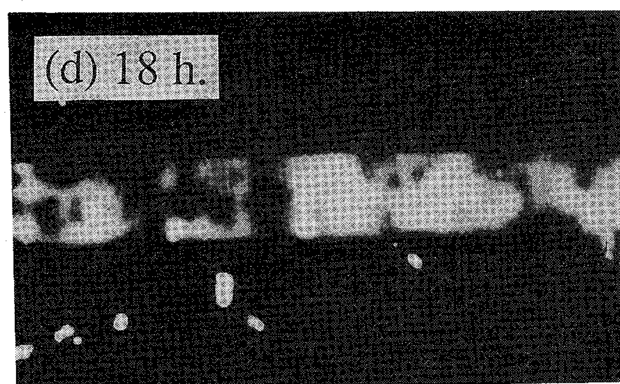

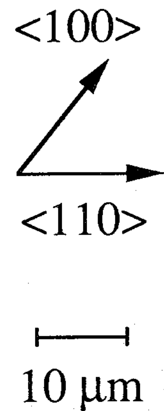

Fig. 3.15. Typical magnified EL topographs of the post-growth annealed AlGaAs/$In_{0.07}Ga_{0.93}As$ laser on Si after (a) 4 min, (b) 1, (c) 6 and (d) 18 h under dc operation at a constant current density of 1.5 kA/cm^2 and temperature of 20 °C.

caused by the complete suppression of <100> DLD growth due to the dislocation pinning and the slow <110> DLD growth associated with REDG motion by stress[9,51] (as shown in Fig. 3.5). In particular, the absence of <100> DLDs suggests that the REDC motion[9,51] which causes rapid degradation is effectively suppressed in the annealed $In_{0.07}Ga_{0.93}As$ active layer. The more increasing lifetime of the AlGaAs/InGaAs laser on Si can be expected to be achieved by suppression of the <110> DLD growth. This will be realized by use of the stress-compensated structure[55-60] such as InGaAs compressive-stress active layer sandwiched by GaAsP tensile-stress confining layers.

3.6 Conclusions

The characteristics of AlGaAs/InGaAs SQW lasers on Si with InGaAs ILs have been studied. The residual stress in the active layer was relatively estimated by use of the degree of polarization. An $AlGaAs/In_{0.02}Ga_{0.98}As$ laser on Si with InGaAs IL has a stress-relieved active layer, while an $AlGaAs/In_{0.07}Ga_{0.93}As$ laser on Si with InGaAs IL has a compressive-stress induced active layer. Compared with a conventional AlGaAs/GaAs laser on Si, the value of J_{th} was reduced for an $AlGaAs/In_{0.02}Ga_{0.98}As$ laser due to the increase of η_i and β. The $AlGaAs/In_{0.07}Ga_{0.93}As$ laser exhibited higher J_{th} than that of the $AlGaAs/In_{0.02}Ga_{0.98}As$ laser because of the reduction of η_i by the increased bending of threading dislocation in the active layer. The lifetimes under APC operation at room-temperature were remarkably increased for these lasers, which resulted from the reduction of DSD by the introduction of InGaAs IL and the reduction of <100> DLD growth velocity by the dislocation pinning in the InGaAs active layer. Furthermore, for

these post-growth annealed lasers, the drastically increased lifetimes were realized. In particular, the longest lifetime was ~24 h for the annealed AlGaAs/$In_{0.07}Ga_{0.93}As$ laser, which was caused by completely suppressed <100> DLD growth and slow <110> DLD growth.

References

1) D. P. Bour, N. A. Dinkel, D. B. Gilbert, K. B. Fabian and M. G. Harvey, IEEE Photon. Technol. Lett., **2**, 153 (1990).

2) A. Larsson, S. Forouhar, J. Cody and R. J. Lang, IEEE Photon. Technol. Lett., **2**, 307 (1990).

3) J. P. van der Ziel and N. Chand, Appl. Phys. Lett., **58**, 1437 (1991).

4) S. E. Fischer, R. G. Waters, D. Fekete, J. M. Ballantyne, Y. C. Chen and B. A. Soltz, Appl. Phys. Lett., **54**, 1861 (1989).

5) D. P. Bour, D. B. Gilbert, K. B. Fabian, J. P. Bednarz and M. Ettenberg, IEEE Photon. Technol. Lett., **2**, 173 (1990).

6) M. Okayasu, M. Fukuda, T. Takeshita and S. Uehara, IEEE Photon. Technol. Lett., **2**, 689 (1990).

7) R. G. Waters, D. P. Bour, S. L. Yellen and N. F. Ruggieri, IEEE Photon. Technol. Lett., **2**, 531 (1990).

8) S. L. Yellen, R. G. Waters, Y. C. Chen and B. A. Soltz, Electron. Lett., **26**, 2083 (1990).

9) R. G. Waters, Prog. Quantum Electron., **15**, 153 (1991).

10) K. Fukagai, S. Ishikawa, K. Endo and T. Yuasa, Jpn. J. Appl. Phys., **30**, L371 (1991).

11) M. Okayasu and M. Fukuda, J. Appl. Phys., **72**, 2119 (1992).

12) S. L. Yellen, A. H. Shepard, R. J. Dalby, J. A. Baumann, H. B. Serreze, T. S. Guido, R. Soltz, K. J. Bystrom, C. M. Harding and R. G. Waters, IEEE J. Quantum Electron., **QE-29**, 2058 (1993).

13) P. A. Kirkby, IEEE J. Quantum Electron., **QE-11**, 562 (1975).

14) H. Ehrenreich and J. P. Hirth, Appl. Phys. Lett., **46**, 668 (1985).

15) H. K. Choi, C. A. Wang and N. H. Karam, Appl. Phys. Lett., **59**, 2634 (1991).

16) H. Sohn, E. R. Weber, J. Tu and S. Wang, *Mat. Res. Soc. Symp. Proc.*, **202**, 609 (1991).

17) J. W. Matthews and A. E. Blakeslee, J. Cryst. Growth, **27**, 118 (1974).

18) R. People and J. C. Bean, Appl. Phys. Lett., **47**, 322 (1985).

19) T. Egawa, Y. Hasegawa, T. Jimbo and M. Umeno, *19th Int. Symp. Gallium Arsenide and Related Compounds*, (Karuizawa, 1992) Inst. Phys. Conf. Ser., **129**, 815 (1993).

20) Y. Hasegawa, T. Egawa, T. Jimbo and M. Umeno, Jpn. J. Appl. Phys., **32**, 175 (1993).

21) T. Egawa, Y. Hasegawa, T. Jimbo and M. Umeno, *Mat. Res. Soc. Symp. Proc.*, **281**, 357 (1993).

22) Y. Hasegawa, T. Egawa, T. Jimbo and M. Umeno, The Review of Laser Engineering, **22**, 977 (1994) (in Japanese).

23) D. T. Cassidy and C. S. Adams, IEEE J. Quantum Electron., **QE-25**, 1156 (1989).

24) H. P. Lee, X. Liu and S. Wang, Appl. Phys. Lett., **56**, 1014 (1990).

25) P. D. Colbourne and D. T. Cassidy, IEEE J. Quantum Electron., **QE-27**, 914 (1991).

26) T. Tanbun-Ek, N. A. Olsson, R. A. Logan, K. W. Wecht and A. M. Sergent, IEEE Photon. Technol. Lett., **3**, 103 (1991).

27) P. D. Colbourne and D. T. Cassidy, IEEE J. Quantum Electron., **QE-29**, 62 (1993).

28) T. Tanaka, H. Yanagisawa, S. Kawanaka and S. Minagawa, IEEE Photon. Technol. Lett., **7**, 136 (1995).

29) S. F. Fang, K. Adomi, S. Iyer, H. Morkoc, H. Zabel, C. Choi and N. Otsuka, J. Appl. Phys., **68**, R31 (1990).

30) H. P. Lee, X. Liu and S. Wang, J. Vac. Sci. Technol., B **8**, 343 (1990).

31) X. Liu, H. P. Lee and S. Wang, Appl. Phys. Lett., **57**, 1955 (1990).

32) D. C. Hall, N. Holonyak, Jr., D. G. Deppe, M. J. Ries, R. J. Matyi, H. Shichijo and J. E. Epler, J. Appl. Phys., **69**, 6844 (1991).

33) G. F. Burns and C. G. Fonstad, IEEE Photon. Technol. Lett., **4**, 18 (1992).

34) K. J. Beernink, P. K. York and J. J. Coleman, Appl. Phys. Lett., **55**, 2585 (1989).

35) C. A. Wang and H. K. Choi, IEEE J. Quantum Electron., **QE-27**, 681 (1991).

36) J. J. Coleman and K. J. Beernink, J. Appl. Phys., **75**, 1879 (1994).

37) N. Wada, S. Sakai and M. Fukui, Jpn. J. Appl. Phys., **33**, 976 (1994).

38) L. B. Freund, J. Appl. Phys., **68**, 2073 (1990).

39) T. Ohori, T. Eshita, S. Miyagaki, K. Kasai and J. Komeno, J. Cryst. Growth, **145**, 924 (1994).

40) M. Mittelstein, Y. Arakawa, A. Larsson and A. Yariv, Appl. Phys. Lett., **49**, 1689 (1986).

41) Y. Arakawa and A. Yariv, IEEE J. Quantum Electron., **QE-22**, 1887 (1986).

42) A. R. Adams, Electron. Lett., **22**, 249 (1986).

43) E. Yablonovitch and E. O. Kane, J. Lightwave Technol., **6**, 1292 (1988).

44) D. Ahn and T.-K. Yoo, Appl. Phys. Lett., **60**, 548 (1992).

45) E. P. O'Reilly and A. R. Adams, IEEE J. Quantum Electron., **QE-30**, 366 (1994).

46) E. Yablonovitch and E. O. Kane, J. Lightwave Technol., **4**, 504 (1986).

47) I. Suemune, IEEE J. Quantum Electron., **QE-27**, 1149 (1991).

48) T. Egawa, Y. Hasegawa, T. Jimbo and M. Umeno, Jpn. J. Appl. Phys., **31**, 791 (1992).

49) Y. Hasegawa, T. Egawa, T. Jimbo and M. Umeno, Jpn. J. Appl. Phys., **34**, 2994 (1995).

50) P. M. Petroff and R. L. Hartman, J. Appl. Phys., **45**, 3899 (1974).

51) O. Ueda, J. Electrochem. Soc., **135**, 11C (1988).

52) H. L. Tsai and J. W. Lee, Appl. Phys. Lett., **51**, 130 (1987).

53) R. W. Kaliski, C. R. Ito, D. G. Mclntyre, M. Feng, H. B. Kim, R. Bean, K. Zanio and K. C. Hsieh, J. Appl. Phys., **64**, 1196 (1988).

54) T. Nishioka, Y. Itoh, M. Sugo, A. Yamamoto and M. Yamaguchi, Jpn. J. Appl. Phys., **27**, L2271 (1988).

55) B. I. Miller, U. Koren, M. G. Young and M. D. Chien, Appl. Phys. Lett., **58**, 1952 (1991).

56) C. P. Seltzer, S. D. Perrin, M. C. Tatham and D. M. Cooper, Electron. Lett., **27**, 1268 (1991).

57) G. Zhang and A. Ovtchinnikov, Appl. Phys. Lett., **62**, 1644 (1993).

58) C. P. Seltzer, S. D. Perrin, M. J. Harlow, R. Studd and P. C. Spurdens, Electron. Lett., **30**, 227 (1994).

59) T. Toyonaka, M. Sagawa, K. Hiramoto, K. Shinoda, K. Uomi and A. Ohishi, Electron. Lett., **31**, 198 (1995).

60) S.-H. Park, W.-G. Jeong and B.-D. Choe, Appl. Phys. Lett., **66**, 201 (1995).